J.E.N.477
Sp ISSN 0081-3397

SELF-SIMILAR ISENTROPIC IMPLOSIONS

by

Rodríguez Manuel
Liñán Amable

Trabajo realizado por la E.T.S. de Ingenieros Aeronauticos de la Universidad Politécnica de Madrid, bajo contrato con el Instituto de Estudios Nucleares.

JUNTA DE ENERGIA NUCLEAR

MADRID, 1980

SELF-SIMILAR ISENTROPIC IMPLOSIONS

by

M. Rodríguez and A. Liñán

E.T.S.I. Aeronáuticos
Universidad Politécnica de Madrid
Madrid - Spain.

ABSTRACT

The self-similar compression of an isentropic spherical gas pellet is analyzed for large values of the ratio of the final to initial densities. An asymptotic analysis provides the solution corresponding to a prescribed value of the final density when it is high. In addition an approximate solution is given when the specific heat ratio, γ, is not constant. The time evolution of the pressure on the outer surface leading to the self-similar solution, is calculated for large density ratios.

INDEX

I. INTRODUCTION

We consider in this note that an initially uniform sphere (or cylinder) of an ideal gas is subjected to a varying external pressure leading to a self-similar isentropic converging compression of the gas. This implies that no shocks will be formed before the wave front arrives at the center of symmetry (r=0). At this moment (taken as t=0), an outgoing shock is formed leaving behind a compressed central hot spot. A description of this isentropic self-similar motion and a numerical analysis is given in Ref. 1. Other kind of isentropic solutions are described in Refs. 2,3. The isentropic imploding motion is of interest in relation with Laser-Fusion, when Deuterium-Tritium pellets are to be compressed isentropically to large densities in a short period of time in order to minimize the laser energy input. In this paper we describe the asymptotic form of this self-similar motion for large values of the ratio of final to initial densities.

II. EQUATIONS

The relevant parameters involved in the problem are the initial density, ρ_o, and the initial sound speed, c_o. The initial radius, r_i, and the time when the compression starts, t_i, enter only through the ratio $(r_i/t_i)=-c_o$. Under these conditions, if the specific heat ratio γ is constant, it is possible to find a self-similar solution of the Euler equations of

motion involving the variables,[4-6]

$$\lambda = \frac{r}{c_o t} \quad , \tag{1}$$

$$R(\lambda) = \frac{\rho}{\rho_o} \quad , \tag{2}$$

$$Z(\lambda) = \left(\frac{ct}{r}\right)^2 \quad , \tag{3}$$

$$V(\lambda) = \frac{ut}{r} \quad , \tag{4}$$

associated with the radius r, density ρ, sound velocity c, radial velocity u and time t. In terms of these variables, the equations describing the motion take the form,

$$\frac{dZ}{dV} = \frac{Z}{V} \frac{2Z-2(1-V)^2+j(\gamma-1)V(1-V)}{(j+1)Z-(1-V)^2} \quad , \tag{5}$$

$$\frac{d(\ln R)}{dV} = \frac{j(1-V)}{(j+1)Z-(1-V)^2} \quad , \tag{6}$$

$$\lambda^2 Z = K R^{(\gamma-1)} \quad , \tag{7}$$

where K is a constant that changes its value only at the outgoing shock, and can be calculated from the initial conditions. In order to obtain the evolution with time of a spherical material surface, $r_p(t)$, which is initially at r_i, we must add the equation,

$$\frac{d[\ln(r_p/r_i)]}{dV} = \frac{1}{1-V} \frac{Z-(1-V)^2}{(j+1)Z-(1-V)^2} \quad . \tag{8}$$

The wave front, converging to the origin with the ve-

locity c_o, is given by $\lambda=-1$. At, and inside, the front $\rho=\rho_o$, $c=c_o$ and $u=0$; therefore, $R=1$, $Z=1$ and $V=0$. With these initial conditions we obtain $K=1$ for the implosion stage.

III. SOLUTION

The solution of the problem is reduced to a single first order ordinary differential equation for $Z(V)$, Eq. (5), which can be integrated numerically; $R(V)$ and the remaining quantities can be obtained by quadratures afterwards. The behaviour of the solution can be understood from the analysis of the singular points of (5) in the phase-plane (V,Z). In Fig. 1 the discontinuous trajectory AOC'-D'E represents a typical integral. The arc AO corresponds to $t<0$; OC'-D'E corresponds to $t>0$ and the jump C'-D' represents the outgoing shock wave. The point B (V^*,Z^*),

$$V^* = \frac{2}{2+(j+1)(\gamma-1)} , \qquad Z^* = \frac{(j+1)(\gamma-1)^2}{\left[2+(j+1)(\gamma-1)\right]^2} \qquad (9)$$

is a saddle point of the differential equation, and the trajectory through it divide the V-Z plane in four regions which correspond to different flow regimes. In order to avoid convergent shocks, the integral curve must lie within the sector ABO. In this sector an infinite number of integrals can exist because the points A and O are nodal ones. Close to the nodal point O, representing the fluid state at $t=0$, $V^2=M_\infty^2 Z$, and the Mach number M_∞, constant in the flow field, identifies each solution.

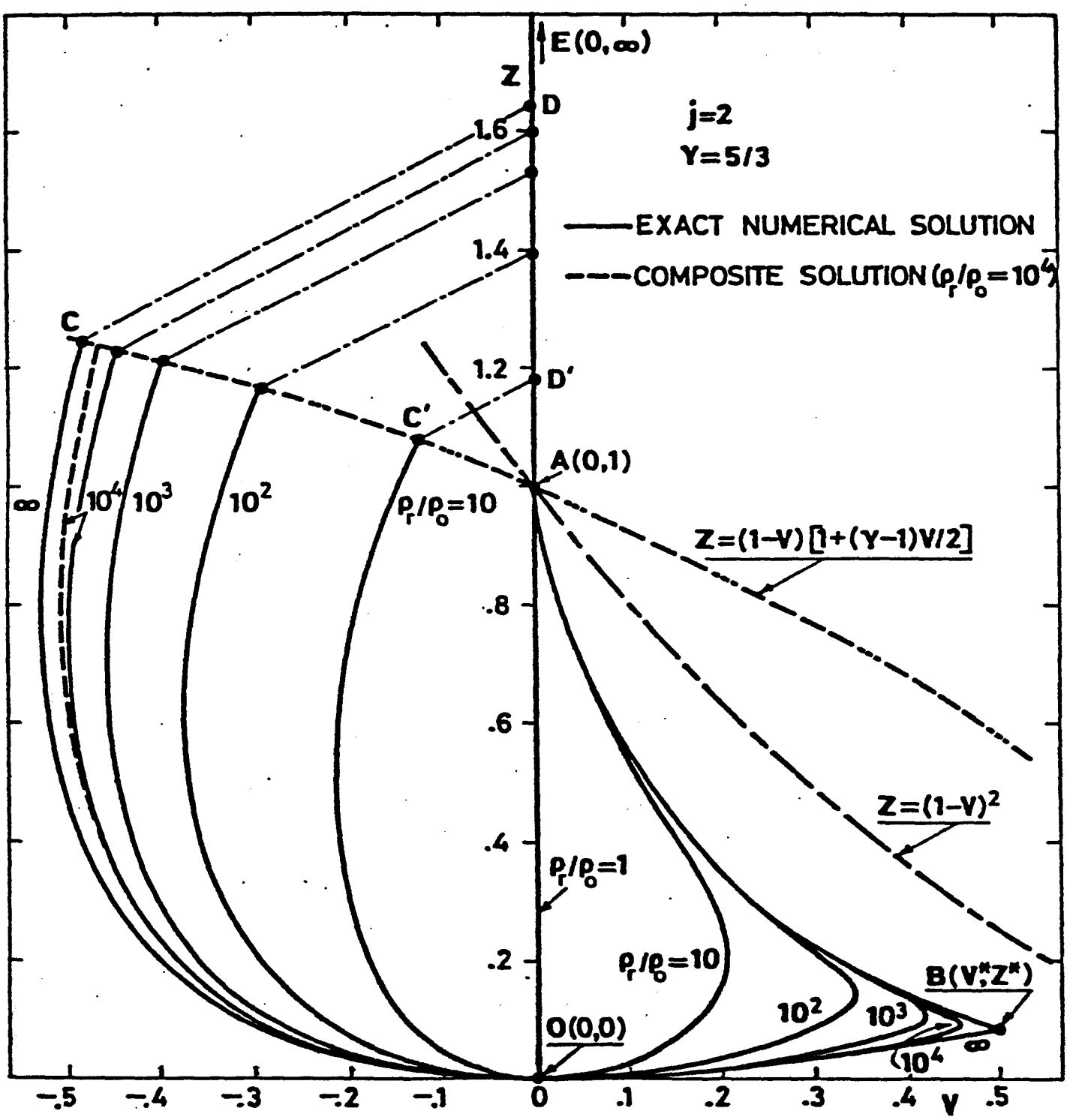

Fig. 1. Integral curves in the phase-plane V-Z for different values of the dimensionless final density ρ_r/ρ_o. $\Gamma=5/3$ and $j=2$.

The limit integral curve, which is discontinuous at the saddle point B (with two branches AB and BOC), corresponds to the limiting value M_∞=3, 1.723 and 1.289 for planar (j=0), cylindrical (j=1) and spherical (j=2) symmetries respectively, and heat specific ratio γ=5/3. When these limit branches are followed, an infinite density is obtained when the point B is reached, at the end of branch AB, and all the mass of the pellet is concentrated at the center of the sphere. The limit branch AB has also been calculated in Refs. 3,7; the solution near B coincides with one of the exact solutions of the Euler equations of motion given by Kidder.[2]

The point C', representing the state of the fluid just before it is reached by the outgoing shock, belongs to the parabola $Z=(1-V)\left[1+(\gamma-1)V/2\right]$, because the fluid behind is left at rest.[5]

The initial point of the integration, point A, being a nodal one, there are different solutions depending on the different ways to start the integration at A. Each solution can be characterized by a maximum value, V_m, of V (see Fig. 1), or a value of M_∞, or a value of the final density $R_r=\rho_r/\rho_o$.

We shall now look for an asymptotic solution for large values of the final density R_r, that implies small values of the ratio $(V^*-V_m)/V^*$. As V_m will be close to V^*, the solution trajectory in the V-Z phase-plane will be close to the limit branches AB and BOC (Fig. 1). Only in the vicinity of B the solution

will differ from the limit branches, and the detailed description of this region will be necessary in order to obtain the prescribed value of the final density.

The numerical solutions corresponding to the two limit branches AB and BOC can be evaluated by integration of the differential Eqs. (5)-(8), starting at B with the asymptotic behaviour,

$$Z = Z^* - \alpha_1 \left(\frac{R}{R_o}\right)^{\mu_1} , \tag{10}$$

$$V = V^* - \left(\frac{R}{R_o}\right)^{\mu_1} , \tag{11}$$

$$\frac{r_p}{r_i} = \frac{r_o}{r_i} \left(\frac{R}{R_o}\right)^{-1/(j+1)} , \tag{12}$$

when we are calculating the solution for branch AB; and,

$$Z = Z^* - \alpha_2 \left(\frac{R}{\hat{R}_o}\right)^{\mu_2} , \tag{13}$$

$$V = V^* - \left(\frac{R}{\hat{R}_o}\right)^{\mu_2} , \tag{14}$$

$$\frac{r_p}{r_i} = \frac{\hat{r}_o}{r_i} \left(\frac{R}{\hat{R}_o}\right)^{-1/(j+1)} , \tag{15}$$

when calculating the branch BOC. The negative constants α_1 and μ_1 and the positive constants α_2 and μ_2, that depend on Υ and j, are given in the Appendix. The two constants R_o and (r_o/r_i) in Eqs. (10)-(12) appear in the numerical solution only as additive constants for the variables lnR and $\ln(r_p/r_i)$, and they can be obtained for different Υ and j from the conditions

$R=(r_p/r_i)=1$ at point A. Also, in Eqs. (13)-(15) two constants, $\hat{R}_o$ and $(\hat{r}_o/r_i)$, are involved, which are additive for the numerical solution for branch BOC; the relations $(R/\hat{R}_o)_C$ and $(r_p/\hat{r}_o)_C$, as well as the values of $V=V_C$ and $Z=Z_C$, should be obtained from the numerical integration when arriving at point C of the parabola $Z_C=(1-V_C)\left[1+(\gamma-1)V_C/2\right]$.

The asymptotic solution near B can be obtained by writing the differential Eqs. (5)-(8) in terms of the variables $(V-V^*)$, $(Z-Z^*)$ and R. After linearization, the differential equations can be integrated to yield,

$$V - V^* = -\left[\left(\frac{R}{a}\right)^{\mu_1} + \left(\frac{R}{b}\right)^{\mu_2}\right] \quad , \tag{16}$$

$$Z - Z^* = -\left[\alpha_1\left(\frac{R}{a}\right)^{\mu_1} + \alpha_2\left(\frac{R}{b}\right)^{\mu_2}\right] \quad , \tag{17}$$

$$\frac{r_p}{r_i} = \left(\frac{R}{d}\right)^{-1/(j+1)} \quad , \tag{18}$$

where the constants of integration a, b and d will be calculated by matching of (16)-(18) with the solutions for the two branches. The matching of (16) and (17) with (10) and (11), where $R/b<<1$, give us $a=R_o$, and with (13) and (14), where $R/a>>1$, gives $b=\hat{R}_o$. In the same way, matching (18) with (12) and (15), leads, to

$$d = R_o\left(\frac{r_o}{r_i}\right)^{(j+1)} = \hat{R}_o\left(\frac{\hat{r}_o}{r_i}\right)^{(j+1)} \quad . \tag{19}$$

The jump shock conditions relate the density at point C, R_C, with the final density, R_r,

$$R_C = R_r/(1-V_C) \quad . \tag{20}$$

Once the values of R_o, (r_o/r_i), $(R/\hat{R}_o)_C$ and $(r_p/\hat{r}_o)_C$ are known by numerical integration of both branches (they are given in Table I for $\gamma=5/3$ and $j=1, 2$), we can obtain the values of $\hat{R}_o$ and $(\hat{r}_o/r_i)$, as a function of the final density, R_r, from (19) and (20),

$$\hat{R}_o = \frac{R_r}{1-V_C} \left(\frac{\hat{R}_o}{R}\right)_C \quad , \tag{21}$$

$$\frac{\hat{r}_o}{r_i} = \frac{r_o}{r_i} \left[(1-V_C) \frac{R_o}{R_r} \left(\frac{R}{\hat{R}_o}\right)_C\right]^{1/(j+1)} \quad ; \tag{22}$$

also, the radius of the pellet at point C is given, according to the mass conservation equation, by

$$\left(\frac{r_p}{r_i}\right)_C = R_r^{-1/(j+1)} \quad . \tag{23}$$

Once the constants involved in (16)-(18) have thus been obtained, the asymptotic solution near B is known and the asymptotic description of the fluid flow is completed for a prescribed value of the final density R_r when it is high.

It is interesting to note that, in first approximation the flow field in the intermediate stage can be obtained if we substitute $V=V^*$ and $Z=Z^*$ into the definition of the self-similar variables (Eqs. (1)-(4)) and in Eq. (7),

$$u = V^* \frac{r}{t} \quad , \tag{24}$$

j	R_o	$(\hat{R}_o/R)_C$	$(\hat{R}_o/R)_D$	r_o/r_i	$(\hat{r}_o/r_p)_C$	V_C
1	1.176×10^{-2}	0.3389	0.1550	14.58	4.015	-1.186
2	1.250×10^{-2}	0.2506	0.1688	5.429	2.280	-0.4822

Table I. Values of the constants R_o, $(\hat{R}_o/R)_C$, $(\hat{R}_o/R)_D$, r_o/r_i, $(\hat{r}_o/r_i)_C$ and the value V_C, which appear in the numerical integration of branches AB and BOC. $\gamma=5/3$ and $j=1,2$.

$$c^2 = Z^*\left(\frac{r}{t}\right)^2 \quad , \tag{25}$$

$$\frac{\rho}{\rho_o} = R = \left[Z^*\left(\frac{r}{c_o t}\right)^2\right]^{1/(\gamma-1)} \quad , \tag{26}$$

This is an exact solution of the Euler equations of motion, corresponding to a flow with constant Mach number $M^*=V^*(Z^*)^{-1/2}$; it is a limit case ($q=1$, $\beta\to\infty$) of one of the solutions given by Kidder,[2] which does not satisfy the initial conditions of uniform density and zero velocity. The trajectory of the outer surface, $r_p(t)$, resulting from (24) is given by,

$$\frac{dr_p}{dt} = V^* \frac{r_p}{t} \quad , \tag{27}$$

so that

$$\frac{r_p}{r_i} = C_1 \left(\frac{t}{t_i}\right)^{V^*} \quad , \tag{28}$$

where C_1 is a constant to be obtained from matching of this solution with the numerical one corresponding to branch AB, or more directly from the law of conservation of mass,

$$\int_o^{r_p} 2j\,\pi\,\rho\, r^j dr = \frac{2j}{j+1}\rho_o\, r_i^{(j+1)} \quad , \tag{29}$$

resulting in the value of C_1 given in the Appendix. The ratio (r_p/r_i) can also be given as function of R in the form,

$$\frac{r_p}{r_i} = \left[\left[1 + \frac{2}{(j+1)(\gamma-1)}\right]\frac{1}{R}\right]^{1/(j+1)} \quad . \tag{30}$$

if we compare this last equation with (12), we obtain a relation between the constants R_o and (r_o/r_i),

$$\frac{r_o}{r_i} = \left[\left[1+\frac{2}{(j+1)(\gamma-1)}\right]\frac{1}{R_o}\right]^{1/(j+1)} , \qquad (31)$$

which can also be used to relate $\hat{R}_o$ and $(\hat{r}_o/r_i)$.

The fluid pressure is in general, given by,

$$\frac{d(\ln p)}{d(\ln \rho)} = \gamma , \quad \frac{p}{p_o} = \exp\left[\int_1^R \frac{\gamma dR}{R}\right] , \qquad (32)$$

and for constant γ,

$$\frac{p}{p_o} = R^{\gamma} , \quad \text{with} \quad \gamma p_o = \rho_o c_o^2 . \qquad (33)$$

Using (28), (30) and (33), we can obtain the pressure -time dependence on the outer surface p_p,

$$\frac{\gamma p_p}{\rho_o c_o^2} = C_2\left(\frac{t}{t_i}\right)^{-\frac{2\gamma(j+1)}{2+(\gamma-1)(j+1)}} , \qquad (34)$$

where C_2 is given in the Appendix.

IV. COMPOSITE SOLUTION

As we have seen, the asymptotic solution is given in terms of two universal numerical solutions corresponding to the two branches AB and BOC and the solution given by (16)-(18) which matches continuously with these two branches. A uniformly valid composite solution can be obtained as follows: Let H be the value of any one of the dependent variables (V, Z or r_p/r_i) corresponding to the composite solution, and let R act as the independent variable. For the composite solution we shall write:

$$H(R) = \frac{H_S \times H_I \times H_B}{H_{SB} \times H_{IB}} \quad , \tag{35}$$

where the subscripts indicate: S = limit branch AB; I = limit branch BOC; B = asymptotic solution near B (16)-(18); SB and IB = = limit branches near B (10)-(15). For values of R/R_r going asymptotically to zero, we are on branch AB; H_B tends to H_{SB} and H_I tends to H_{IB} and, therefore, H(R) tends to H_S. When R/R_r is of order unity we are on branch BOC and H_S tends to H_{SB}, H_B to H_{IB} and H(R) tends to H_I. However, it is interesting to note that if R_r tends to infinity $(H_{SB} \times H_{IB})/H_B$ tends to V^* and Z^* for V and Z respectively, and to the value given in (30) for r_p/r_i, so that,

$$V(R) = \frac{V_S(R) \times V_I(R)}{V^*} \quad , \tag{36}$$

$$Z(R) = \frac{Z_S(R) \times Z_I(R)}{Z^*} \quad , \tag{37}$$

$$\frac{r_p(R)}{r_i} = \left[\frac{r_p(R)}{r_i}\right]_S \times \left[\frac{r_p(R)}{r_i}\right]_I \times \left[\frac{(j+1)(\gamma-1)R}{2+(j+1)(\gamma-1)}\right]^{\frac{1}{j+1}} \quad , \tag{38}$$

and, therefore, the asymptotic solution near B is not needed to obtain the composite solution in first approximation. Nevertheless, the analytical description of this region is necessary in order to understand how matching between the two branches takes place.

Notice that when calculating the composite solution given by (35) or (36)-(38), the values of all the H's must be

evaluated at the same value of $R \in [1, R_c]$. This implies that the numerical integration of the branches should be started on A (for branch AB) and on B (for branch BOC) simultaneously. As the numerical integration of branch AB is unstable when the integration is started on A, we must perform previously the numerical integration of this branch from B to a point close to A, for which R is close to 1 and then proceed backwards towards B.

V. RESULTS

A uniformly valid asymptotic description of the self-similar isentropic compression of a spherical or cylindrical pellet of uniformly initial density is given by (35) or (36)-(38), for large values of the ratio of final to initial densities. The composite solution (35) is written in terms of two universal numerical solutions, corresponding to the limiting branches AB and BOC in the phase-plane V-Z of Fig. 1, that are represented in Figs. 2 and 3. The constants R_o and r_o/r_i appearing in (36)-(38) are functions of γ and j, and they are given in the Appendix for $\gamma=5/3$; the constants $\hat{R}_o$ and $\hat{r}_o/r_i$ appearing in H_I are functions of γ, j and the final density R_r given by (21) and (22).

Density profiles as function of λ, obtained directly from the numerical integration of branches AB and BOC, are plotted in Fig. 4. The value of R tends to infinity (or zero),

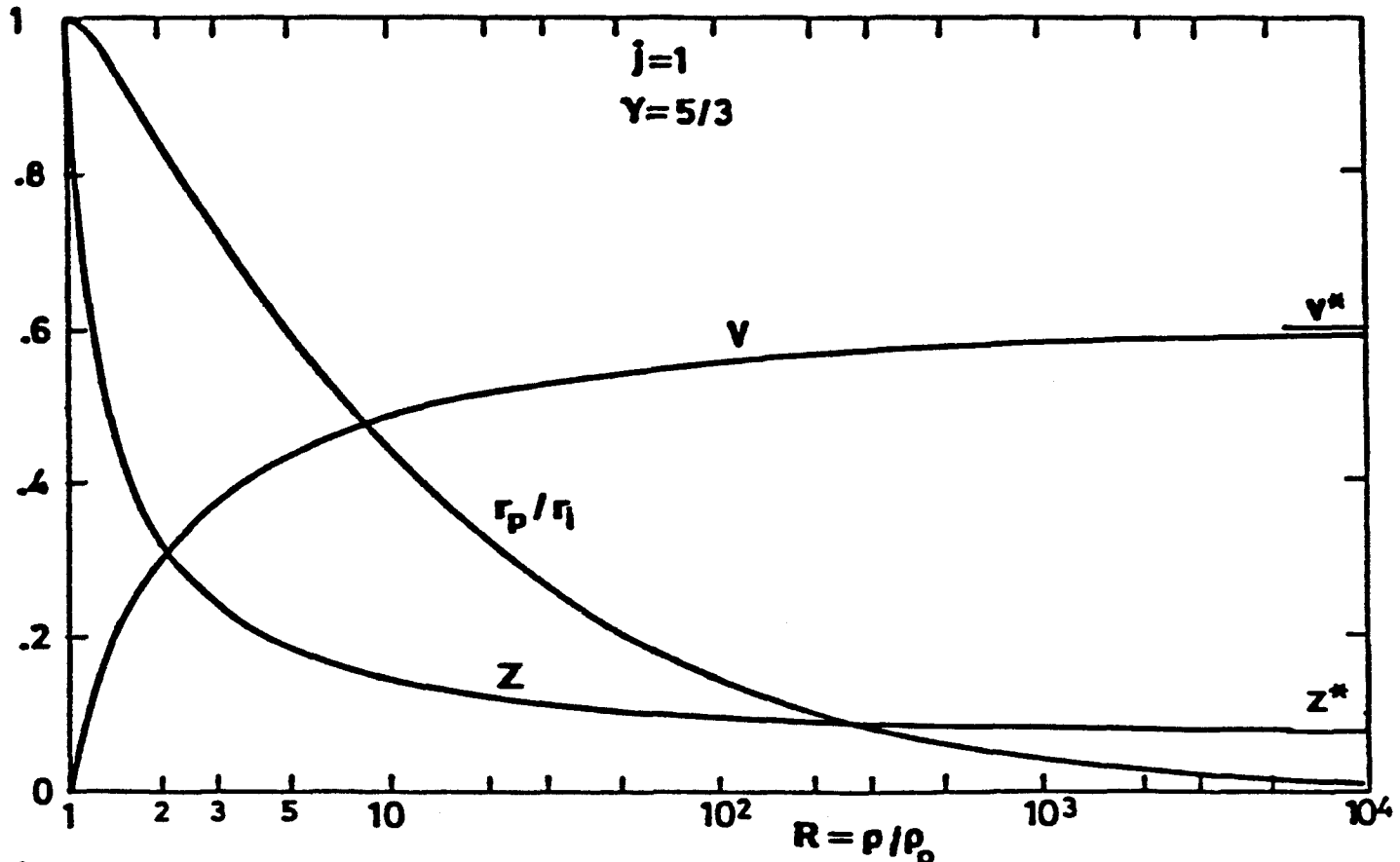

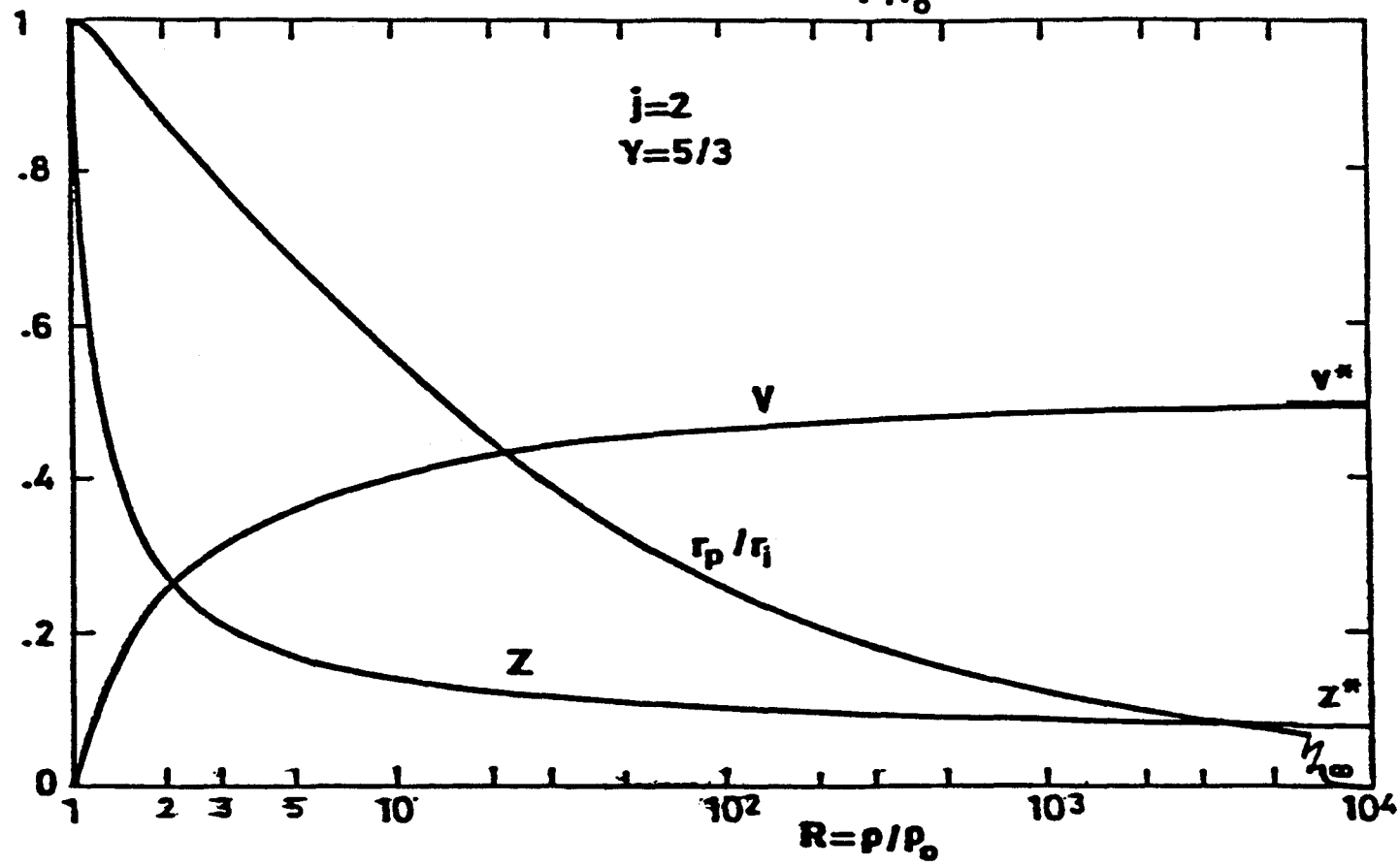

Fig. 2. Values of the self-similar variables V and Z and the dimensionless outer radius r_p/r_j vs. dimensionless density $R=\rho/\rho_o$ corresponding to the branch AB. $\gamma=5/3$ and $j=1,2$.

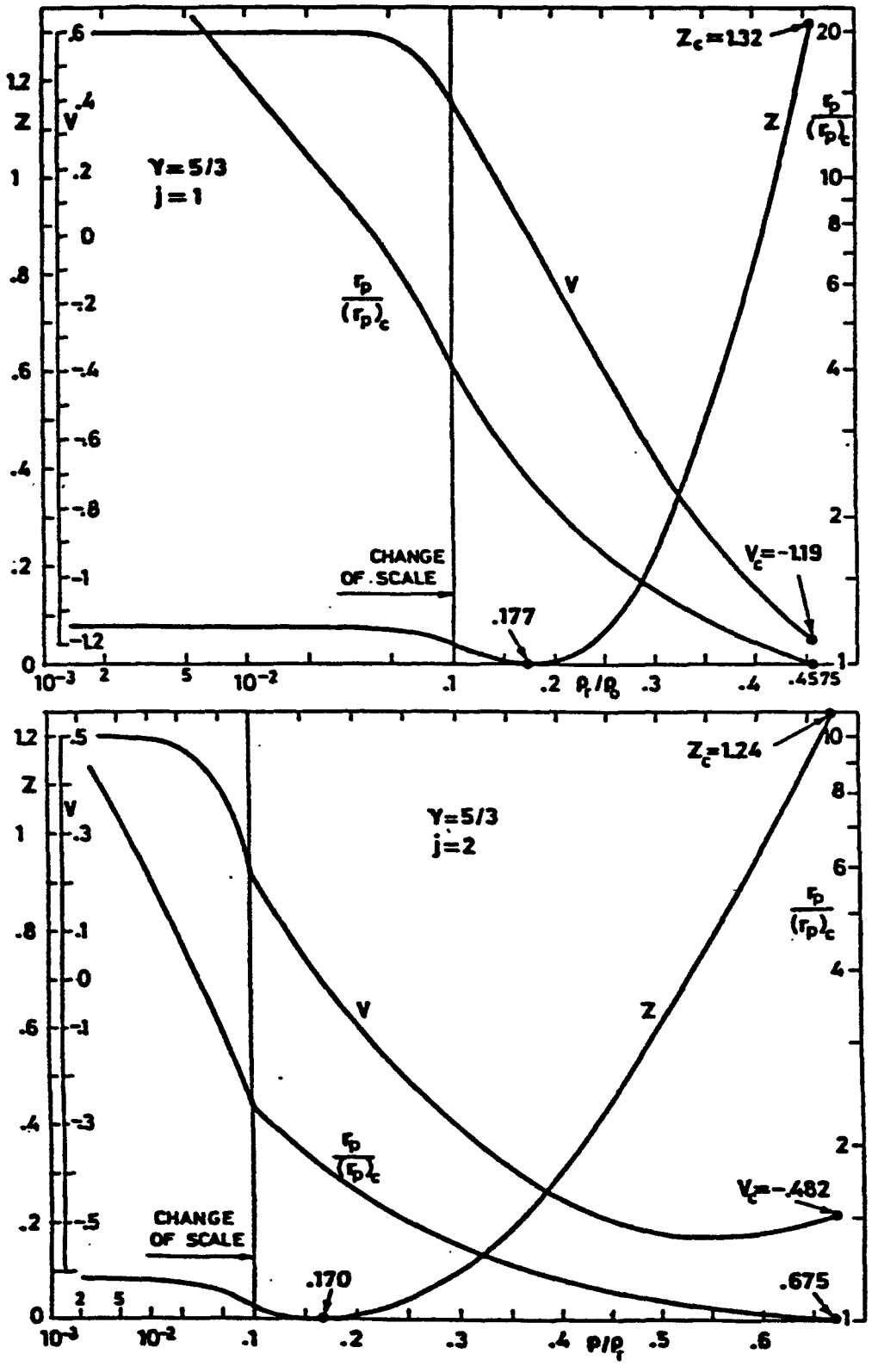

Fig. 3. Values of the self-similar variables V and Z and the ratio $r_p/(r_p)_c$ vs. the ratio ρ/ρ_r corresponding to the branch BOC. Y=5/3 and j=1,2.

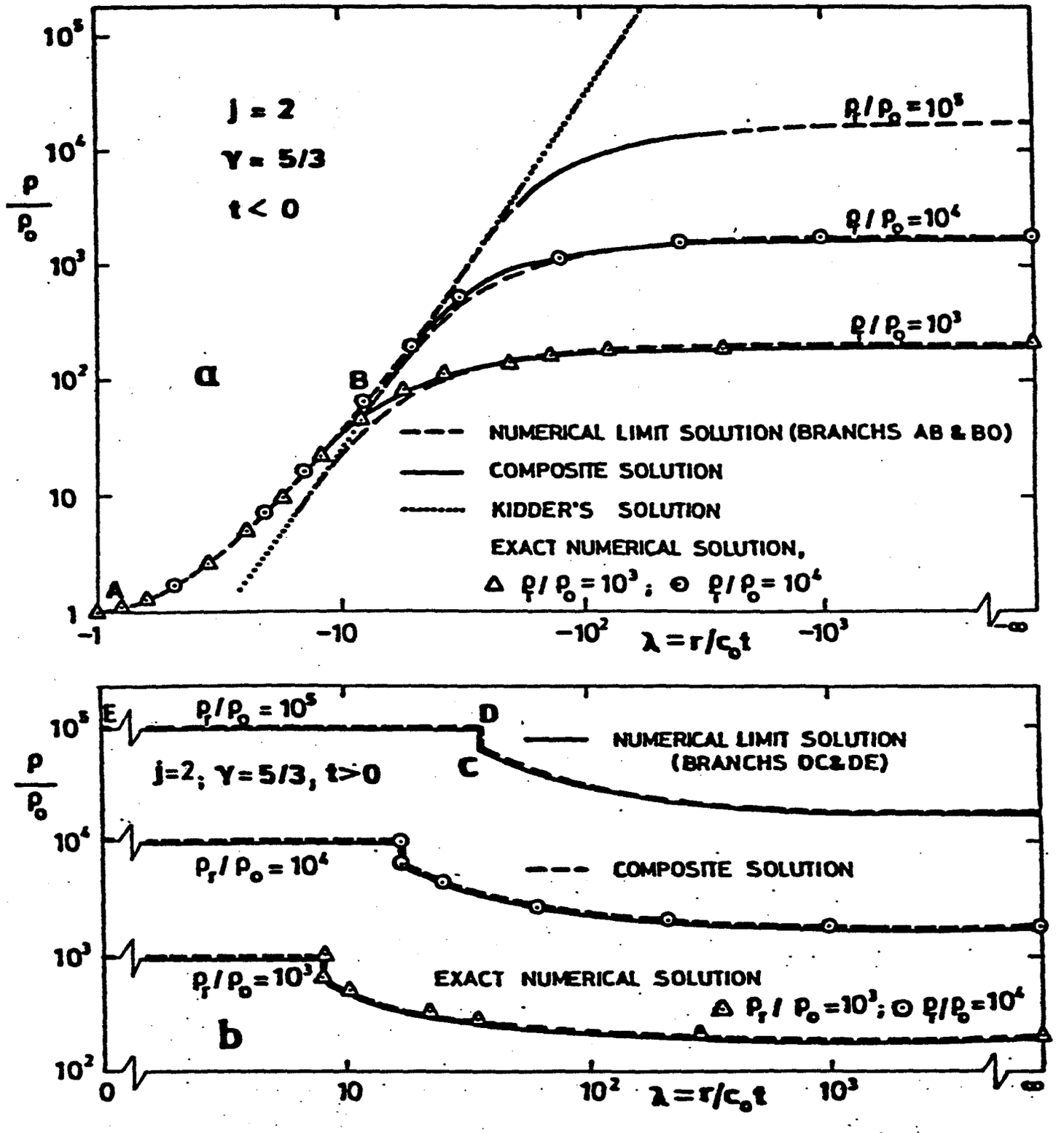

Fig. 4. Dimensionless density ρ/ρ_o vs. $\lambda=r/c_o t$ for different values of the dimensionless final density ρ_r/ρ_o. $\gamma=5/3$ and $j=2$.

when approaching the point B along the branch AB (or BOC), following the common asymptote: $R^{(\gamma-1)}=Z^*\lambda^2$, that corresponds to the Kidder's solution. The aditive constants (in a log-log plott) appearing in the solution for branch BOC are determined graphically to insure matching with the AB solution by sliding the curve BO, maintaining the asymptote KK, until the final density ρ_r/ρ_o is reached. In this way the asymptotic solution is described graphically in terms of the asymptotic solution for an initial stage (or region) AB, the Kidder's solution for an intermediate stage, and the solution BOC for the final stage, that includes an outgoing shock that leaves the pellet at a uniform density. We have also plotted in Fig. 4, for comparison, the exact numerical solution and the composite solution given by (36)-(38). Notice that for large values of the ratio ρ_r/ρ_o most of the density increment takes place during the intermediate stage, which is described by Kidder's solution; the density changes only by a factor of order unity during the first and the final stages.

Fig. 5 shows the trajectory of the outer surface of the pellet as well as the density profiles for two typical times, as described by the exact and asymptotic solutions.

The non-dimensional pressure,

$$\frac{\gamma p_p(t)}{\rho_o c_o^2} = R^{\gamma}(t) \quad , \tag{39}$$

and the non-dimensional power input,

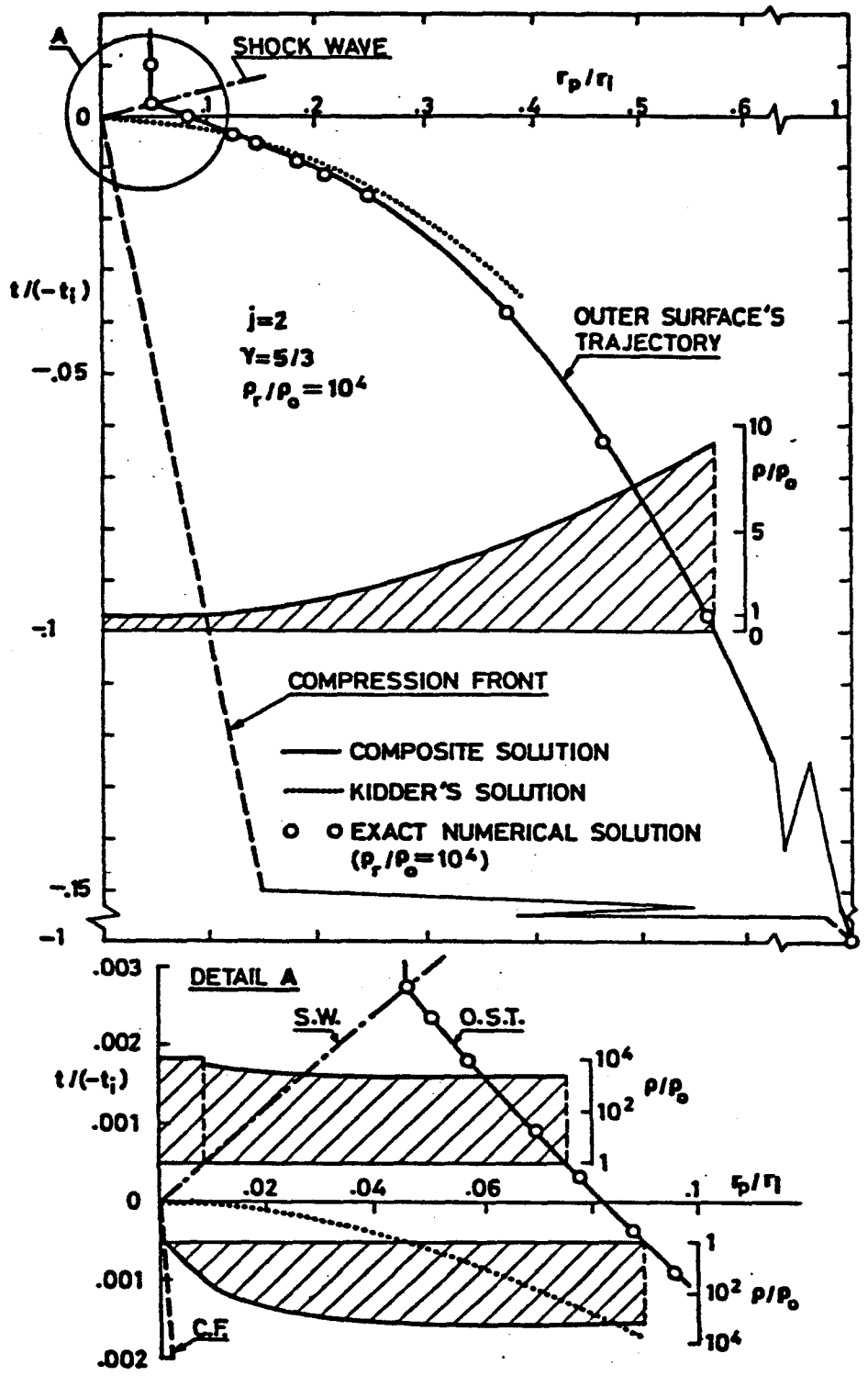

Fig. 5. Dimensionless outer radius r_p/r_i vs. dimensionless time $t/(-t_i)$ and dimensionless density ρ/ρ_o vs. r_p/r_i at different times. Y=5/3, j=2 and $\rho_r/\rho_o=10^4$.

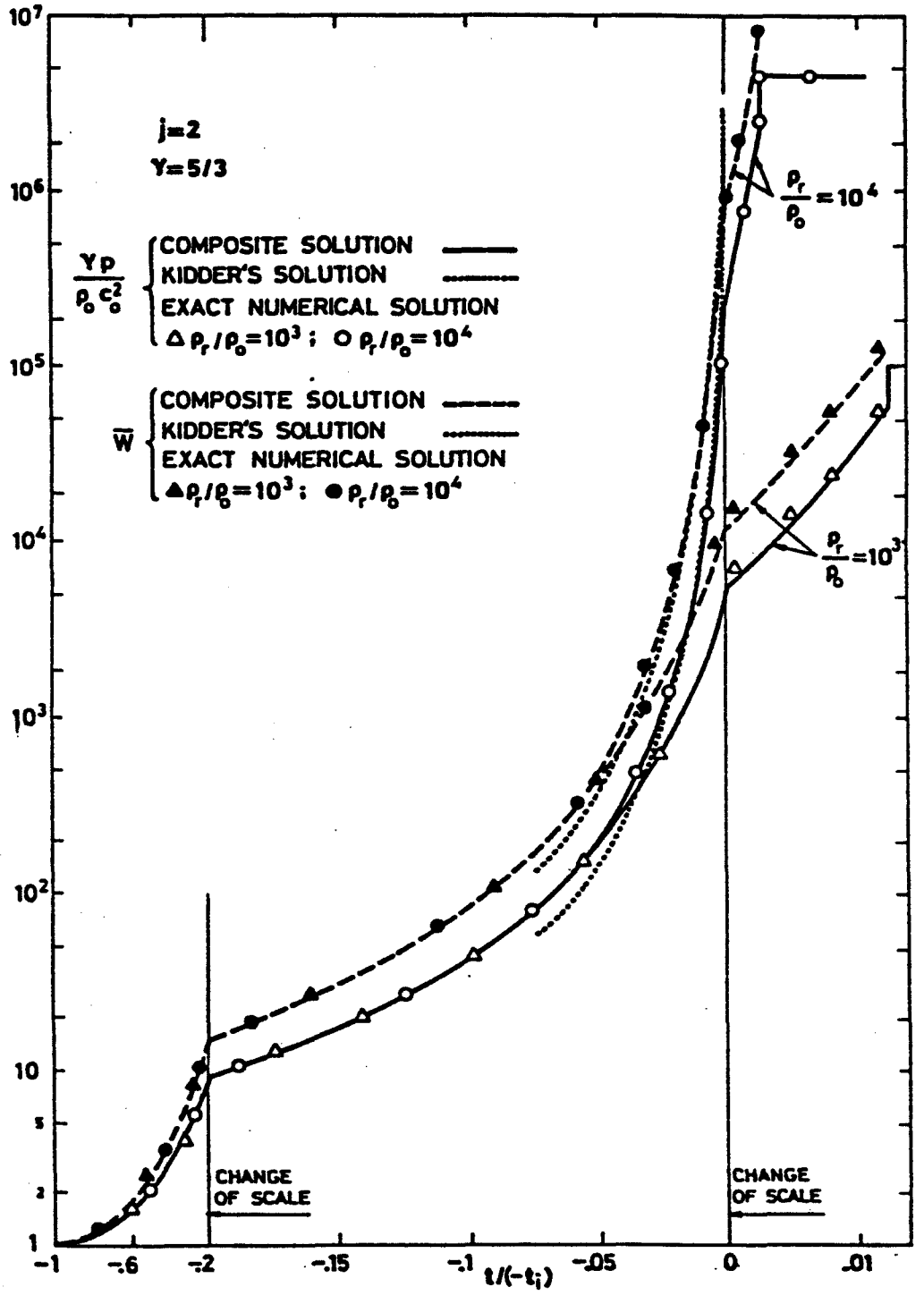

Fig. 6. Dimensionless pressure on the outer surface and dimensionless laser power vs. dimensionless time. Y=5/3. j=2 and $\rho_r/\rho_o=10^3$, 10^4.

$$\overline{W} = \frac{16WZ_i}{25\pi}\, r_i^{-j} \left(\frac{n_c m_i}{p_o^3}\right)^{1/2} = \left(\frac{r_p}{r_i}\right)^j \left(\frac{p_p}{p_o}\right)^{3/2} , \qquad (40)$$

on the outer surface required to produce the self-similar isentropic implosion, have been represented in Fig. 6 for two final densities (10^3 and 10^4 times the initial). Eq. (40) has been obtained using the analysis of the thin deflagration regime given by Barrero and Sanmartín,[9] where the region of electron heat conduction is considered to be quasi-steady and very thin compared with the pellet radius. There W is the laser power, Z_i and m_i are the atomic number and mass of the ions of the ablator, n_c is the critical electron density associated with the laser frequency. We can see in Fig. 6 that in a first stage the required pressure history is independent of the final value of the density. This stage corresponds to the branch AB. Most of the increment in surface pressure takes place following the simplified description of the intermediate stage, given by Kidder's solution, until a leveling to the final pressure, associated with the final density, takes place according to the asymptotic solution for the final stage. If the surface pressure does not follow the history given in this figure, for example, if the pressure pulse is suddenly stopped at a certain time, the solution will not be self-similar resulting in expansion waves that will lower the average density within the pellet.

The Euler equations of motion have an exact self-similar isentropic solution only for a constant value of γ.

However, if the resulting changes in density are large, significant changes in γ may take place in most of the applications. We shall show now how the results of our asymptotic analysis can be used to account for the effects of variable $\gamma(\rho,S_o)$, if the derivative $\varepsilon=\partial\gamma/\partial(\ln\rho)$ at constant entropy is small compared with unity; that is, when ρ must change by a large factor to produce changes in γ of order unity.

In the first stage we found that ρ changes by a factor of order unity and therefore γ may be replaced by γ_o with relative errors of order ε; similarly the changes in ρ from ρ_c in the final stage are also given by a factor of order unity and, thus, γ can be approximated by γ_c ($\gamma_c=5/3$ for large densities[8]) with errors of order ε. The important changes in ρ and therefore in γ take place in the intermediate stage (or intermediate region of the flow field), where it is easy to show that (24)-(26) and (28) with variable $V^*(\gamma)$, $Z^*(\gamma)$, $C_1(\gamma)$ and $\gamma(\rho,S_o)$, are solutions of the Euler equations if terms of order ε are neglected.

A uniformly valid composite solution can be written by generalizing (36)-(38) to account for variable γ, as

$$V(\gamma,R)=\frac{V_S(\gamma_o,R)\times V_I(\gamma_c,R)\times V^*(\gamma)}{V^*(\gamma_o)\times V^*(\gamma_c)}\,, \qquad (41)$$

$$Z(\gamma,R)=\frac{Z_S(\gamma_o,R)\times Z_I(\gamma_c,R)\times Z^*(\gamma)}{Z^*(\gamma_o)\times Z^*(\gamma_c)}\,, \qquad (42)$$

$$\left[\frac{r_p(\gamma,R)}{r_i}\right] = \left[\frac{r_p(\gamma_o,R)}{r_i}\right]_S \times \left[\frac{r_p(\gamma_c,R)}{r_i}\right]_I \times$$

$$\times \left\{\frac{(j+1)(\gamma_o-1)(\gamma_c-1)\left[2+(j+1)(\gamma-1)\right]R}{(\gamma-1)\left[2+(j+1)(\gamma_o-1)\right]\left[2+(j+1)(\gamma_c-1)\right]}\right\}^{\frac{1}{j+1}} \qquad (43)$$

where $V^*(\gamma)$ and $Z^*(\gamma)$ are given in (9).

In addition, when we are interested in obtaining the numerical solution of (5)-(8) for a precribed value of the final density, we do not have, in general, a relation between the initial point of integration (points A and 0 are nodal ones) and the prescribed final density and, therefore, we must proceed by an iterative method. With the asymptotic solution given by (16)-(18) we have a method to relate the point were V takes it maximum value (V_m,Z_m), which can be used as initial point of the numerical integration, with the final density R_r when it is high. This relation is obtained from (16) together with dV/dR=0 at $V=V_m$, so that,

$$V^*-V_m = \frac{\mu_2-\mu_1}{\mu_2}\left\{\left(-\frac{\mu_1}{\mu_2}\right)\left[\frac{R_r}{(1-V_c)R_o}\left(\frac{\hat{R}_o}{R}\right)_c\right]^{\mu_2}\right\}^{\frac{\mu_1}{\mu_2-\mu_1}}, \qquad (44)$$

and from (6) we obtain

$$Z_m = \frac{(1-V_m)^2}{j+1} \quad . \qquad (45)$$

The relations (44)-(45) between (V_m,Z_m) and the prescribed value

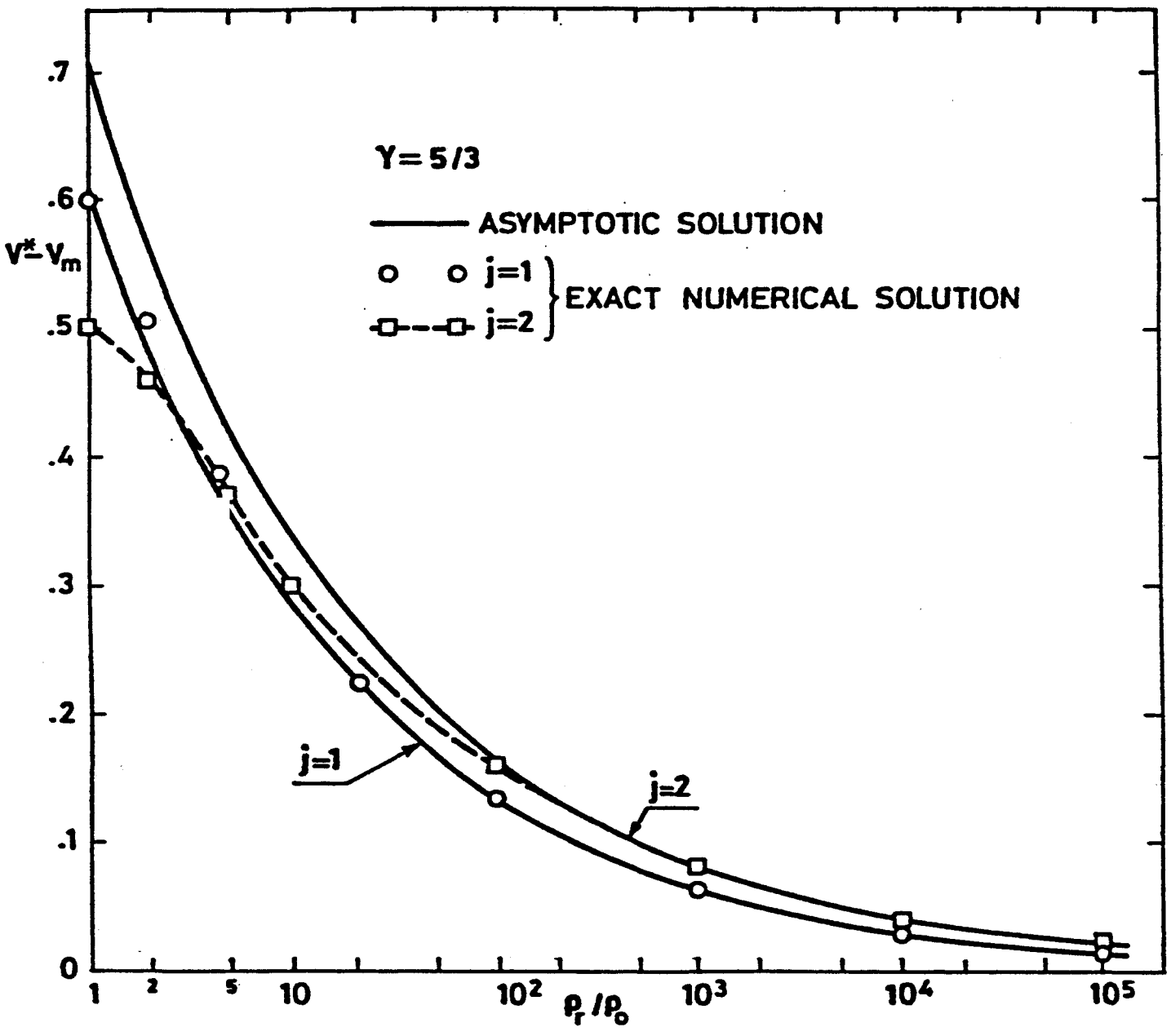

Fig. 7. V^*-V_m vs. dimensionless final density ρ_r/ρ_o. $\gamma=5/3$ and $j=1,2$.

of the final density are only valid asymptotically for large values of R_r, but they can be used with accurate results for moderately large values of the final density, as shown in Fig. 7.

ACKNOWLEDGMENTS

This work was conducted at the Universidad Politécnica de Madrid, Spain, in partial fulfillment of the requirements for the doctoral degree of one of the authors (M.R.).

This research was performed under the auspices of the Junta de Energía Nuclear (JEN) of Spain.

REFERENCES

[1] C. Ferro Fontan, J. Gratton and R. Gratton, Phys. Lett. 55A 1 (1975) 35.

[2] R.E. Kidder, Nucl. Fusion 14 (1974) 53.

[3] D.E.T.F. Ashby, Nucl. Fusion 16 (1976) 231.

[4] R. Courant and K.O. Friedrichs, "Supersonic Flow and Shock Waves" (Interscience, 1948).

[5] L.I. Sedov, "Similarity and Dimensional Methods in Mechanics" (Academic, 1959).

[6] K.P. Stanyukovich, "Unsteady Motion of Continuous Media" (Pergamon, 1960).

[7] M. Rodríguez and A. Liñán, Rept. J.E.N. 405 (1978), Junta de Energía Nuclear, Madrid.

[8] Ya.B. Zel'dovich and Yu.P. Raizer, "Physics of Shock Waves and High-Temperature Hydrodynamic Phenomena" (Academic, 1967).

[9] A. Barrero and J.R. Sanmartín, Phys. Fluid, 21, 1957, (1978).

APPENDIX

The values of $\alpha_{1,2}$ and $\mu_{1,2}$, which appear in Eqs. (10)-(15), are:

$$\alpha_{1,2} = \frac{(\gamma-1)(\gamma-3)}{2[2+(\gamma-1)(j+1)]} \times$$

$$\times \left[1 \pm \left[1 + \frac{8(\gamma-1)(j+1)+2j^2(\gamma-1)^2+2j(\gamma-3)(\gamma-1)}{(\gamma-3)^2}\right]^{1/2}\right] ,$$

$$\mu_{1,2} = \frac{[2+(\gamma-1)(j+1)]\alpha_{1,2}+2(\gamma-1)}{j(\gamma-1)} ,$$

where α_1 is the negative root ($\alpha_1<0$) and α_2 the positive one ($\alpha_2>0$), which correspond to values of $\mu_1<0$ and $\mu_2>0$.

The constants C_1 (Eq. (28)) and C_2 (Eq. (34)) as function of γ and j are given by,

$$C_1 = (j+1)^a \left[1+\frac{2}{(j+1)(\gamma-1)}\right]^{(\gamma+1)a} , \qquad C_2 = \left(Z^* C_1^2\right)^{\frac{\gamma}{\gamma-1}}$$

with,

$$a = \frac{1}{2+(\gamma-1)(j+1)} .$$